

# Imaging Spectroscopic Analysis at the Advanced Light Source

T. WARWICK, S. ANDERS, Z. HUSSAIN, G. M. LAMBLE, G. F. LORUSSO\*, A. A. MACDOWELL, M. C. MARTIN, S. A. MCHUGO, W. R. MCKINNEY, AND H. A. PADMORE

Lawrence Berkeley National Laboratory, Berkeley, CA 94720, USA.

\*Center of X-ray Lithography, University of Wisconsin, Madison, WI, USA

## Introduction

One of the major advances at the high-brightness third-generation synchrotrons is the dramatic improvement of imaging capability. There is a large multi-disciplinary effort under way at the ALS to develop imaging X-ray, UV and infrared spectroscopic analysis on a spatial scale from a few microns to 10 nm. These developments make use of infrared light, ultraviolet light, and X-rays from 100 eV to 10 keV. Imaging and spectroscopy are finding applications to problems in surface science, bulk materials analysis, semiconductor structures, particulate contaminants, magnetic thin films, biology and environmental science.

This article is an overview and status report from the developers of these techniques at the ALS.

## PEEM microscopy at the ALS

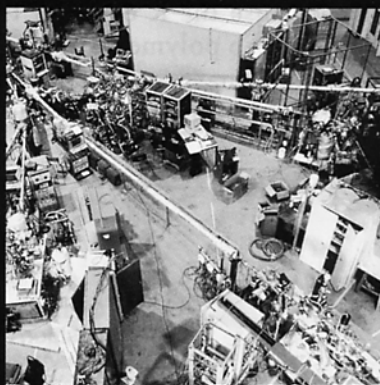
Photoemission electron microscopy (PEEM) using X-rays is a full-field imaging technique based on the secondary-electron emission caused by X-ray absorption. The secondary electrons are imaged by an electron-optics column with a resolution given by the electron optics. By varying the incident X-ray wavelength incrementally one is able to obtain local near-edge X-ray absorption fine structure spectroscopy (NEXAFS) data with high spatial resolution.

There are two PEEM microscopes in operation at the ALS at the moment. The first one, called PRISM, is a two-lens system with a movable aperture in the back focal plane of the objective lens [1]. The electron optics has a spatial resolution of 200 nm. The microscope is described in detail elsewhere [2]. It is located at Beamline 8.0, an undulator beamline with an

energy range of 200 eV to 1500 eV and a resolving power of  $E/\Delta E = 6000$ . The X-rays are focused on the sample by a Kirkpatrick-Baez pair of mirrors into a spot of 200- $\mu\text{m}$  diameter.

A wide variety of materials and systems have been studied using this microscope, including polymers, diamond-like carbon and diamond, various phases of titanium disilicide and of boron nitride, small particles, electron field-emission materials, and ceramics (metal nitrides and

## Your Partner for SYNCHROTRON RADIATION EQUIPMENT



SUPER-ACO - LURE (ORSAY - FRANCE)

Diffraction gratings, Mirrors, Mirror Manipulators, Monochromators and Spectrographs (TGM, PGM, SGM,... DRAGON and PADMORE...). Complete Beamlines for the Far UV and Soft X-Ray.

**From the OPTICAL COMPONENT  
to the COMPLETE BEAMLINE  
through dedicated subassemblies...**

**ISA** **JOBIN YVON - SPEX**  
Groupe HORIBA

16-18 rue du Canal - 91165 Longjumeau Cedex - France  
Tel. : (33) 01 64 54 13 00 - Fax : (33) 01 69 09 93 19

In USA call: (1) 908/494 86 60 - In Netherlands call: (31) 172/477 320  
In Germany call: (49) 89/46 23 17-0 - In Italy call: (39) 2/57 60 30 50  
In UK call: (44) 181/204 81 42

Circle No. 123

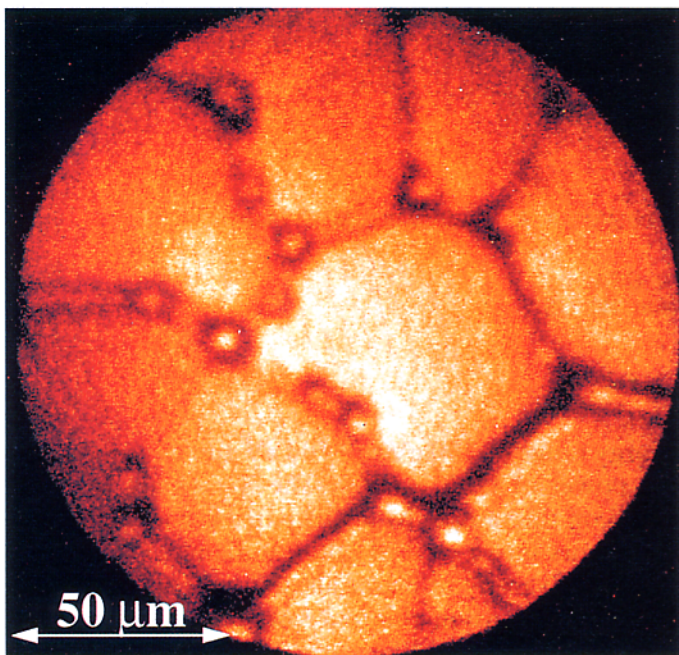


Figure 1. PEEM image of bilayer of PS and PBrS after four days of annealing at 180 °C. Image was acquired at 286.3 eV. The contrast is due to topography, since in the later phase of dewetting the surface is covered completely by PS.

oxides). In the following, a few examples will be given.

Polymers are very suitable systems for X-ray microscopy studies because the K edges of the elements typically present in polymers (C, N, O, F, Br...) show very strong, sharp, and characteristic resonances for determining the chemical

bonding states of the elements [3]. Polymers are used in many technological applications, such as colloid paint systems, thin films for the alignment of liquid crystals in liquid-crystal displays, lubricants on hard disks, photoresist, to name only those applications we have studied so far. We have studied bilayer systems of polystyrene (PS) and brominated polystyrene (PBrS) consisting of a 30-nm-thick PBrS layer on top of a 30-nm-thick PS layer produced by spin casting [4]. The samples were annealed for various durations at 180 °C and studied by scanning transmission electron microscopy (STXM) and PEEM. The formation of spines as a result of the dewetting process of the two polymers was observed with both methods. STXM was used to determine that the spines are composed of brominated polystyrene. The PEEM results showed that the dewetting of the PBrS starts in small areas, exposing the PS underlayer, and in the later phase leads to a complete coverage of the surface with a thin PS film, including the PBrS spines. Figure 1 shows a PEEM image of a sample that was annealed for four days.

In another series of experiments, the tribochemical behavior of lubricants on hard disks after wear and the transport of lubricants to the slider surface was studied [5]. It was found that the perfluoropolyether lubricant on the disk undergoes chemical changes during the wear. Fluorine is removed from the polymer, and oxidation in the form of carboxylic bonds takes

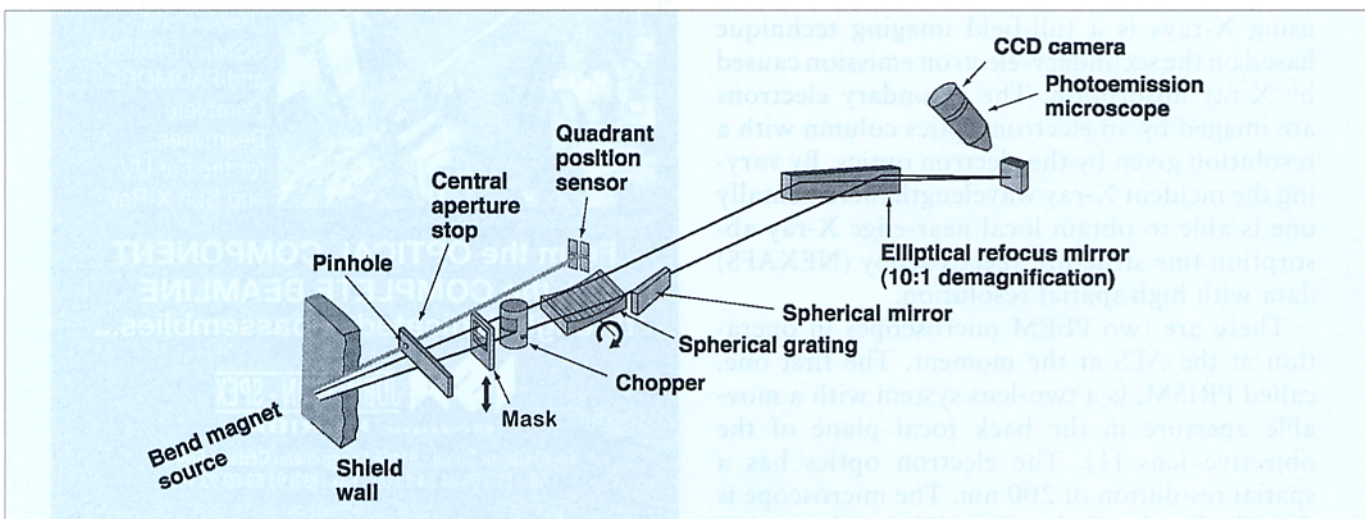
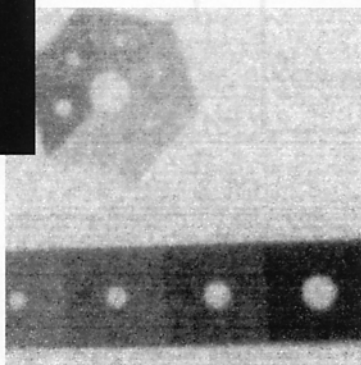
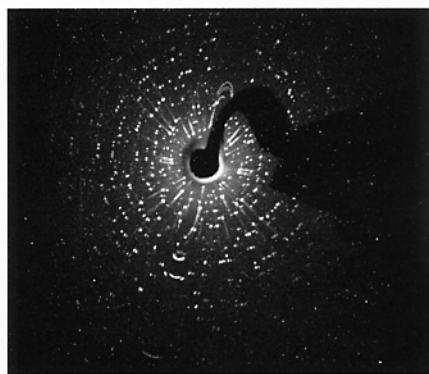


Figure 2. Schematic layout of Beamline 7.3.1.1 at the ALS.

# X-Ray Imaging Systems from Photonic Science

– for Synchrotron Systems, industrial radiography cameras and NDT systems



## Featuring:

- ◆ Fibre optic inputs from 150mm to 70mm, 2042<sup>2</sup> pixels
- ◆ 16, 12 or 10-bit digitization, slow scan or fast readout
- ◆ Intensified high resolution camera – 1024<sup>2</sup> pixels
- ◆ X-Ray Intensifier for 200–800 keV operation with digital camera (wafer tube unaffected by magnetic fields!)

UK Tel: +44 (0) 1580 88099 Fax: +44 (0) 1580 880910  
France Tel: +33 476 93 57 20 Fax: +33 476 93 57 22

email: [info@photonic-science.ltd.uk](mailto:info@photonic-science.ltd.uk)

<http://www.photonic-science.ltd.uk>

Circle No. 136

place. Local NEXAFS spectra taken in wear tracks and on slider surfaces showed that this degraded lubricant is present in wear tracks, but it is also transferred to slider surfaces where it accumulates in particular in scratches at the slider.

The new microscope PEEM2 is installed at the bending-magnet Beamline 7.3.1.1, which provides soft X-rays in the energy range from 250 eV to 1500 eV with a resolving power of  $E/\Delta E = 1800$ . Figure 2 shows a schematic of the beamline. The X-rays are focused to a 30- $\mu\text{m}$  spot on the

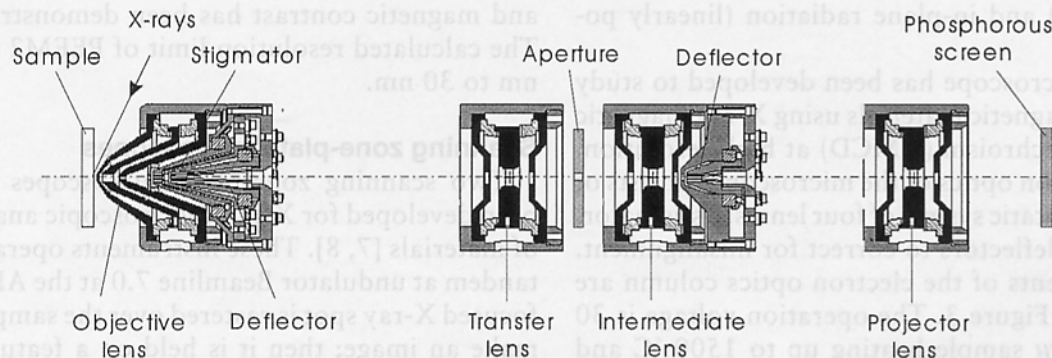


Figure 3. Schematic layout of PEEM2. Part of the lens design was adapted from an existing X-ray transmission microscope [6].

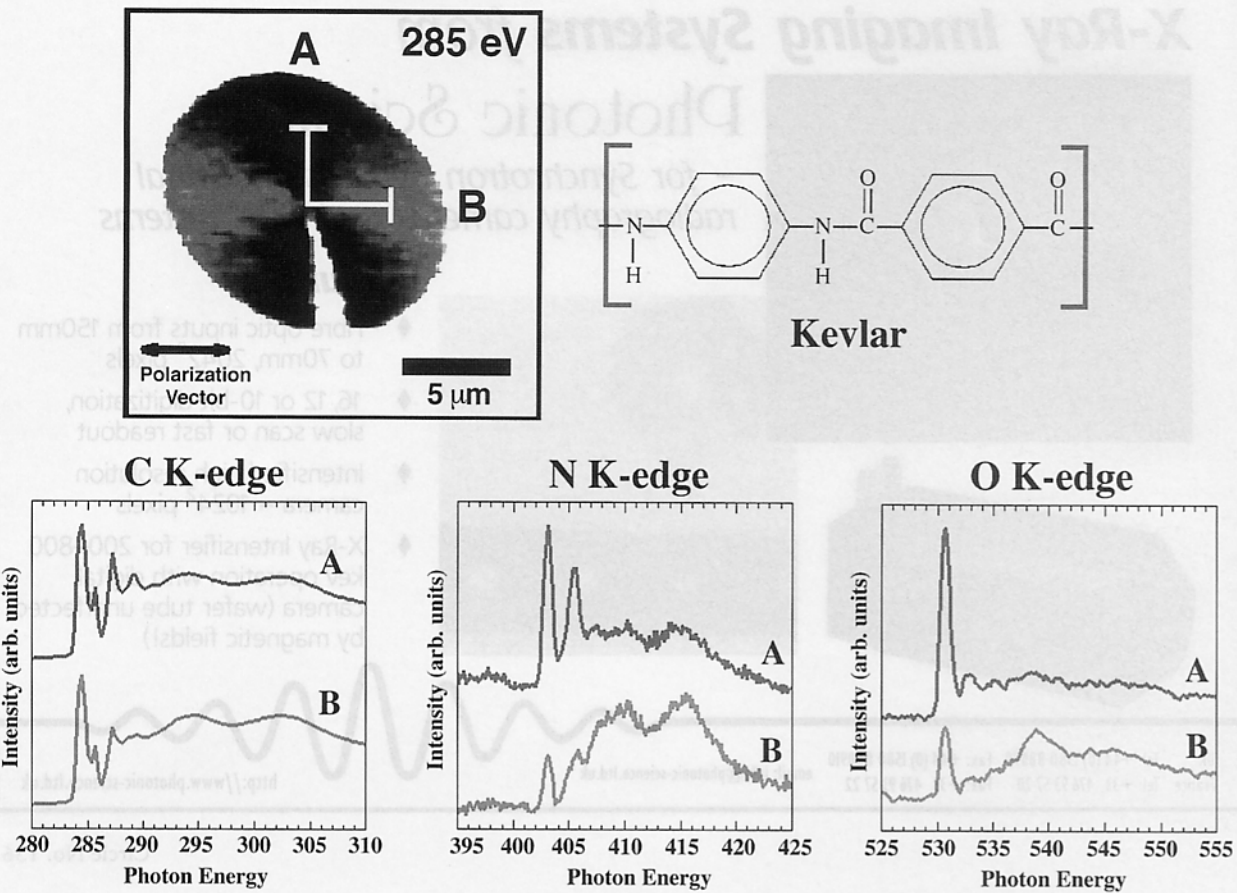


Figure 4. A sectioned Kevlar fiber measured in STXM (results courtesy of H. Ade and A. Garcia). Absorption spectra are measured at point A and B, showing the dependence on the angle between the photon polarization vector (horizontal) and the preferentially tangential orientation of the  $\pi$  bonds of N and O. The polarization contrast reverses between the  $\pi$ - and  $\sigma$ -orbital peaks.

sample. The beamline was designed specifically for XMCD experiments and is equipped with a mask and chopper to select above-plane and below-plane radiation (left and right circularly polarized) and in-plane radiation (linearly polarized).

The microscope has been developed to study mainly magnetic materials using X-ray magnetic circular dichroism (XMCD) at high resolution. The electron optics of the microscope consists of an electrostatic system of four lenses, a stigmator, and two deflectors to correct for misalignment. The elements of the electron optics column are shown in Figure 3. The operation voltage is 30 kV. *In-situ* sample heating up to 1500 °C and film growth is possible. An automated sample-transfer system allows fast sample exchange, and

a sample preparation chamber is equipped with a sputter gun, a heater, and evaporators. The PEEM2 is currently in the commissioning phase. First images have been acquired, and elemental and magnetic contrast has been demonstrated. The calculated resolution limit of PEEM2 is 20 nm to 30 nm.

Scanning zone-plate microscopes

Two scanning zone-plate microscopes have been developed for X-ray spectroscopic analysis of materials [7, 8]. These instruments operate in tandem at undulator Beamline 7.0 at the ALS. A focused X-ray spot is rastered over the sample to make an image; then it is held on a feature of interest for spectral measurements. The count rates in these microscopes are about ten times

higher than previously available. We are presently using zone-plate lenses with a central stop and 80-nm outer zone width, and a corresponding diffraction limit to the spatial resolution of about 100 nm. An order sorting aperture (OSA) is held in front of the sample and precisely positioned on the optical axis ( $\pm 2$  microns) to allow only the first-order diffracted focus to reach the sample. The measured FWHM of the X-ray spot is 130 nm.

The Scanning Transmission X-ray Microscope (STXM) provides imaging NEXAFS analysis of samples in transmission at atmospheric pressure. The transmission geometry is the most efficient use of photons for an absorption spectrum, well suited to radiation-sensitive organic samples [9]. Measurements in transmission are bulk sensitive, so that surface contamination is not a concern; this allows the operation of the microscope at atmospheric pressure, in air or helium, with hydrated samples for problems in environmental science [10, 11]. Circularly polarized photons have been generated and used for imaging domains at the L edge in Fe, Ni, and Co magnetic films [12]. We have measured  $2 \times 10^7$  photons/second with a spectral width 1/3000 in the zone-plate first-order focus spot at 300 eV, with the storage ring running at 1.5 GeV and 400 mA. Figure 4 is from a case study illustrating the ability of STXM to perform polarization-sensitive spectromicroscopy of organic polymers at the K edge of the three most important atomic species-C, N, and O.

The scanning photoelectron microscope (SPEM) provides imaging X-ray photoelectron spectroscopy (XPS) and NEXAFS analysis of sample surfaces in a UHV environment. Here the sample is stationary during imaging and the zone plate is rastered in the illumination field to carry the focused spot across the sample surface. The illumination is of the order of 1-mm diameter and the raster range is  $80 \times 80$  microns. The electron spectrometer can view the entire range of the image area and collects photo-electrons at 60 degrees from the sample normal. The OSA is within 0.5 mm of the sample surface, and the zone-plate assembly is cut back on one side to allow a line of sight for the spectrometer.

NEXAFS capability is included by means of a UHV flexure to carry the zone plate 0.5 mm longitudinally to retain the focus condition as

# DIGITAL X-RAY SPECTROSCOPY

## DXP 4C/4T

1 DETECTOR OR 100

## WITH SO MANY REASONS

### 2X THROUGHPUT OR MORE

76 kcps for 2  $\mu$ s Peaking, 180 kcps input

### EQUAL RESOLUTION

Matches good analog systems

### FULL SPECTRA

At 2X SCA speeds

### MUCH LOWER COST

Save 50% or more

### MUCH MORE COMPACT

Compare our 4 channels to their 1

### EXCELLENT LINEARITY

Integral Nonlinearity < 0.1%

### MUCH LESS PILEUP

By up to factor of 100

### 100 % COMPUTER CONTROL

Gain, peaking times, pileup tests

### PRECISE DEADTIME CORRECTION

$\pm 0.5\%$ , 0-120 kcps at 4  $\mu$ s peaking

### TIME RESOLVED SPECTRA

$\mu$ sec time resolution

### PROCESS SYNCHRONIZED SPECTRA

Phase sensitive collection

### ALLOWS FULL AUTOMATION

with VAX®, LabView®, EPICS®, etc.

## WHY WAIT ?

X  
R  
A  
Y  
**XIA**  
INSTRUMENTATION  
ASSOCIATES

2513 Charleston Road  
Suite 207  
Mountain View, CA  
94043 USA  
Tel: (650) 903-9980  
Fax: (650) 903-9887

<http://www.xia.com>

**X-ray Instrumentation Associates**

Represented in Japan by Seiko-EG&G



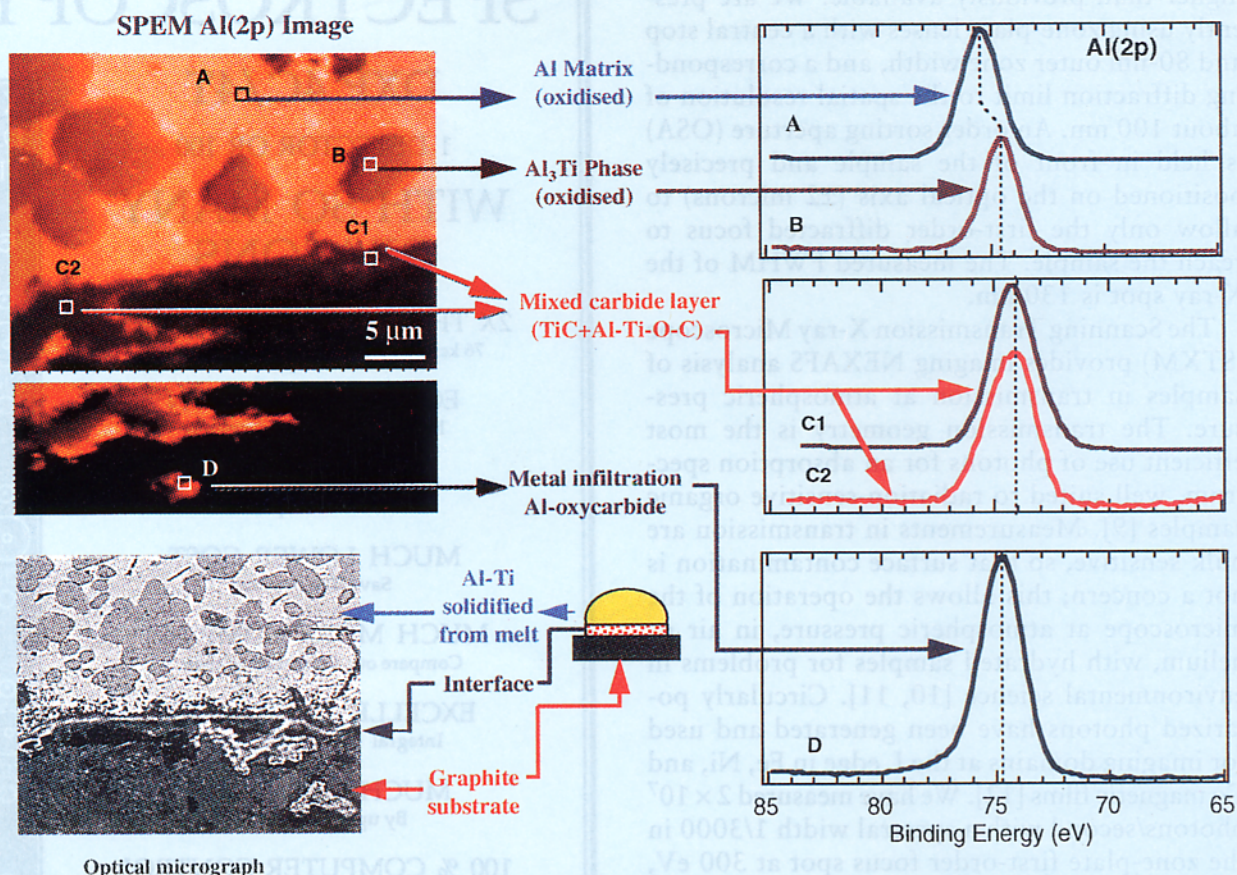


**Figure 5.** A SPEM case study in which an Al/Ti melt has been allowed to solidify on a graphite substrate (results courtesy S. Seal and N. Sobczak). The image of the polished section shows the aluminum metal, precipitates of  $\text{Al}_3\text{Ti}$  alloy, and the graphite interface, with carbide formation. Different core-level chemical shifts are observed from the Al, the  $\text{Al}_3\text{Ti}$  alloy, and the carbide region. In this case, sputtering has removed the adventitious carbon contamination, but the surface is still oxidized.

the photon energy changes. The OSA is fixed to the zone plate in such a way that the focal length is built-in to the assembly. Covering a range of photon energies requires different zone-plate/OSA combinations with varying built-in focal lengths (e.g., 700 eV for survey spectra including oxygen 1s photoelectrons, 270 eV to 310 eV for carbon K-edge NEXAFS measurements). Five zone plates will be mounted together on a monolithic array with precisely parallel optical axes (to  $\pm 1$  mrad), interchangeable under computer control. So far we have operated the microscope with three zone-plate/OSAs aligned in this way.

SPEM allows us to perform quantitative XPS measurements of atomic concentration and core-level chemical shifts over regions of the sample surface as small as the spatial resolution of the

zone plate lens. The zone-plate array can be lowered out of the beam, and the sample surface can be observed with a magnifying video system, allowing visible fiducial marks on the sample to be used to position the region of interest within the  $100 \times 100$  micron range of the scan stage. XPS spectra are measured with typical photopeak count-rates of 70,000 counts/second (Au 4f at 420-eV photon energy).

#### Micro X-ray Photoelectron Spectroscopy on Beamline 7.3.1.2

The MicroXPS beamline has been developed at the ALS, in collaboration with Intel Corporation and Applied Materials, to fulfill the increasingly demanding needs of the semiconductor industry. The use of tunable, high-brightness

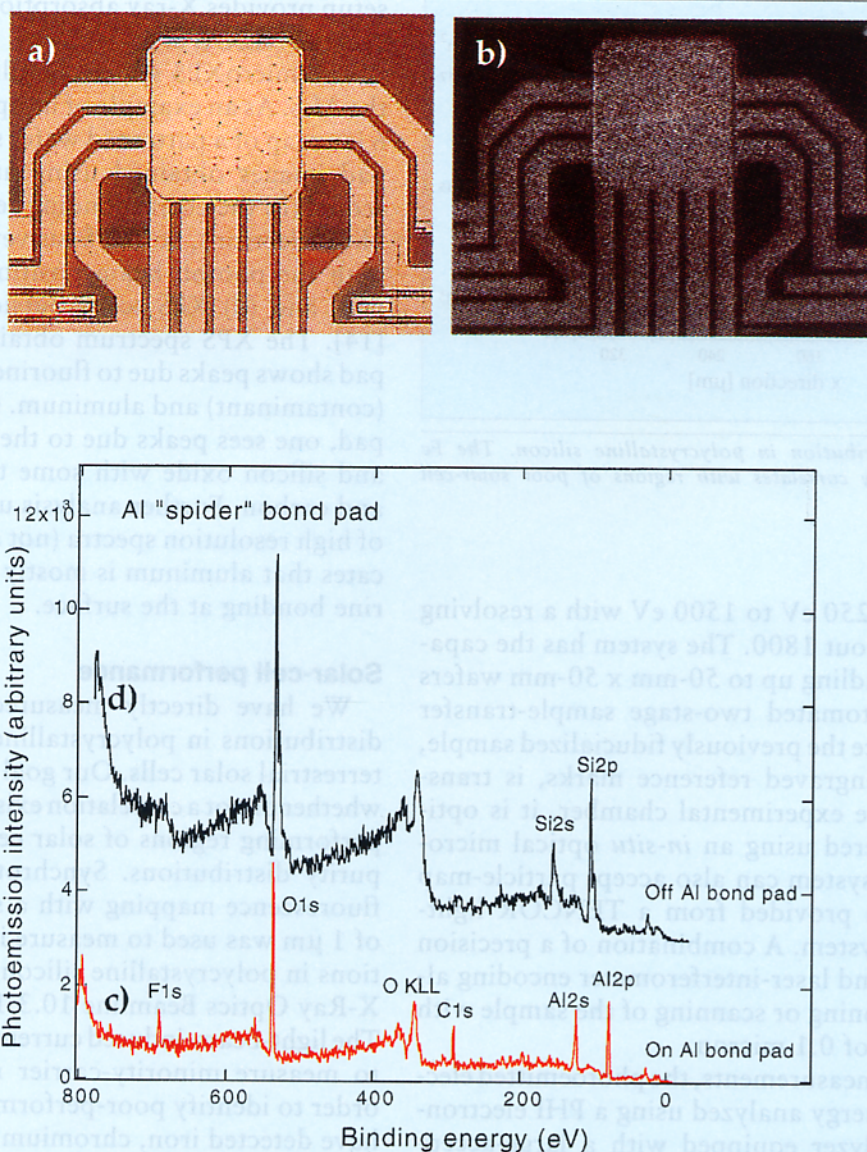
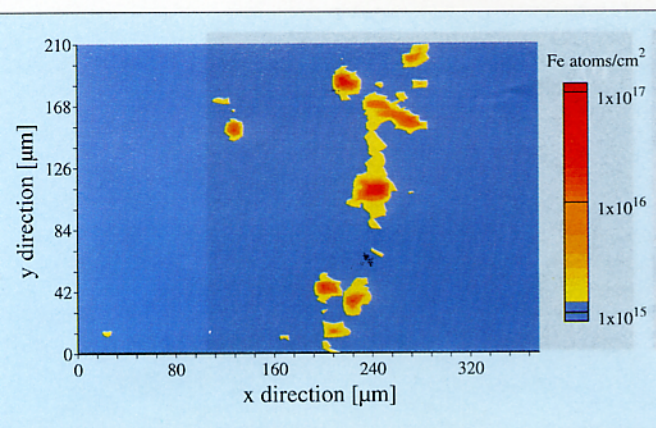


Figure 6. (a) optical image of a patterned wafer (300 microns  $\times$  400 microns); (b) corresponding XPS micrograph image using Al-2p photoelectrons; (c) XPS survey spectrum at the Al bond pad; and (d) outside the bond pad.

synchrotron radiation at micron spatial resolution for X-ray photoelectron spectroscopy provides a technique of choice for mapping the near surface elemental and chemical nature of microstructure in materials. Such a study is essential, for example, for investigation of device-failure mechanisms and for the development of next-generation microelectronics devices.

The optical design of the microXPS system includes a spherical mirror that accepts 0.2 mrad of monochromatized radiation from a bending-

magnet beamline with a simple monochromator and focuses the beam to adjustable cross slits, which constitute the object for the microXPS imaging system. The microfocusing is achieved through a pair of orthogonal elliptical bent mirrors (Kirkpatrick-Baez configuration) to focus the beam down to 1 micron  $\times$  1 micron. These mirrors are made by bending high-strength steel flats polished and edge-shaped to high precision [13]. The total flux deliverable at the sample location is up to  $2 \times 10^{10}$  photons/s in the energy



**Figure 7.** Fe distribution in polycrystalline silicon. The Fe distribution exactly correlates with regions of poor solar-cell performance.

range from 250 eV to 1500 eV with a resolving power of about 1800. The system has the capability of handling up to 50-mm x 50-mm wafers with an automated two-stage sample-transfer facility. Once the previously fiducialized sample, with laser-engraved reference marks, is transferred to the experimental chamber, it is optically registered using an *in-situ* optical microscope. The system can also accept particle-map information provided from a TENCOR light-scattering system. A combination of a precision X-Y stage and laser-interferometer encoding allows positioning or scanning of the sample with a precision of 0.1 micron.

For XPS measurements, the photoemitted electrons are energy analyzed using a PHI electron-energy analyzer equipped with a large-acceptance-angle Omega lens system. The tunability of the synchrotron radiation provides an advantage for carrying out the XPS study using a photon energy chosen to provide a high cross-section for the element of interest and a low cross-section for elements whose signals need to be suppressed. It may also provide some control of depth sensitivity by using the kinetic-energy dependence of the electron escape depth. The system also incorporates a variety of other instrumentation: a standard Al K $\alpha$ /Mg K $\alpha$  X-ray source, a variable-energy ion gun for sputtering and depth profiling, a partial-yield electron detector, and electron flood gun for sample neutralization (it works best in conjunction with low-energy ion source). The same experimental

setup provides X-ray absorption measurements, such as NEXAFS.

The microXPS system is fully operational at the ALS. As an example of its application, Figure 6 is a map of a patterned wafer showing (a) bond pad images obtained using an optical microscope, (b) the corresponding region using Al 2p photoelectrons, (c) XPS survey scans obtained with the photon beam positioned at the bond pad, and (d) XPS scans outside the bond pad [14]. The XPS spectrum obtained on the bond pad shows peaks due to fluorine, oxygen, carbon (contaminant) and aluminum. Outside the bond pad, one sees peaks due to the substrate silicon and silicon oxide with some traces of fluorine and carbon. Further analysis using curve fitting of high resolution spectra (not shown here) indicates that aluminum is mostly involved in fluorine bonding at the surface.

### Solar-cell performance

We have directly measured metal-impurity distributions in polycrystalline silicon used for terrestrial solar cells. Our goal was to determine whether or not a correlation exists between poorly performing regions of solar cells and metal impurity distributions. Synchrotron-based X-ray fluorescence mapping with a spatial resolution of 1  $\mu$ m was used to measure impurity distributions in polycrystalline silicon at the Center for X-Ray Optics Beamline 10.3.1 at the ALS [15]. The light-beam-induced current method was used to measure minority-carrier recombination in order to identify poor-performance regions. We have detected iron, chromium and nickel impurities. Figure 7 denotes the spatial distribution of Fe in the scanned region; Cr and Ni were distributed in the same locations as the Fe. The impurity distribution exactly correlated with poor performing regions in the material. These results indicate metal impurities are the cause for high-carrier-recombination regions in polycrystalline silicon and, therefore, play a significant role in the performance of the material as a solar cell. The results also yields insight for methods of solar-cell improvement.

### Photoemission microscopy with MAXIMUM

In 1987, the University of Wisconsin, in collaboration with the ALS, began the development of an X-ray microscope system of the scanning

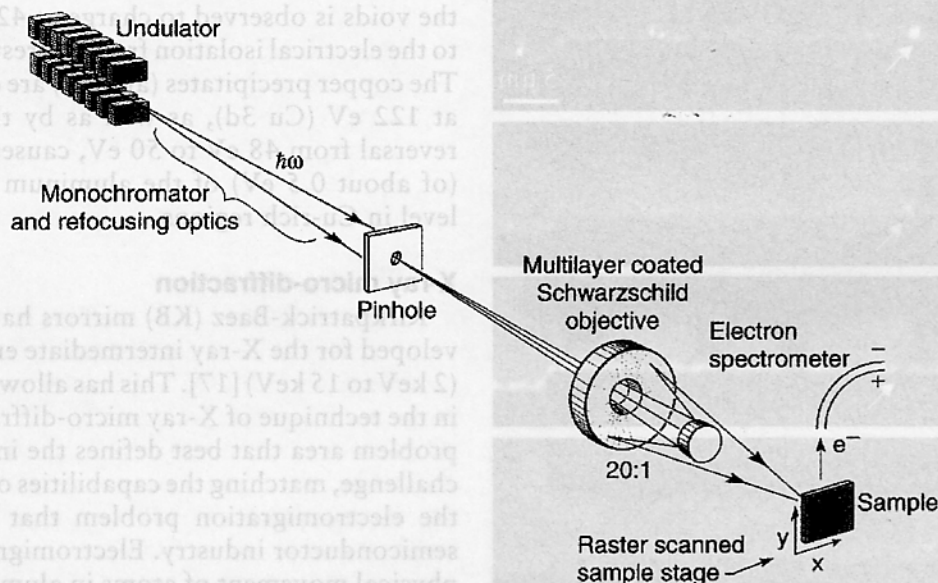


Figure 8. Layout of MAXIMUM at Beamline 12.0 at the ALS.

type with the goal of reaching a spatial resolution better than 0.1 micron and a spectral resolution better than 200 meV, while working at a base pressure better than  $10^{-10}$  torr. All these goals were achieved in 1992, after a period of development of about 5 years in MAXIMUM (Multiple Application X-ray Imaging Undulator Microscope) [16]. Several breakthroughs had to be achieved in order to deliver the required performance. In particular, MAXIMUM mounted the first UHV-compatible Schwarzschild objective with *in-situ* alignment, was used for the first at-wavelength Foucault test in the extreme ultraviolet (EUV), and demonstrated the high efficiency of multilayer optics near the silicon edge.

In MAXIMUM, radiation from the synchrotron source is monochromatized and focused by a Kirkpatrick-Baez (KB) system to illuminate a pinhole, which serves as source for the microscope optics. A multilayer-coated (Ru-B<sub>4</sub>C for operation at 130 eV) Schwarzschild Objective (SO) produces an image of the pinhole with a 20 $\times$  demagnification. When a sample is placed at the focus, photoelectrons are collected by a cylindrical mirror analyzer (CMA) electron spectrometer. The sample is mounted on a scanning stage, and by rastering the sample, it is possible

to produce a two-dimensional photoemission image. Figure 8 is a schematic of MAXIMUM.

The photoemission microscope MAXIMUM was originally installed at the University of Wisconsin (Madison) Synchrotron Radiation Center (SRC). During the period from 1992 to 1995, the microscope was successfully used to study semiconductor surfaces, interfaces, biological samples and organic particles. However, during the operation of the microscope, it became apparent that the microscope performance was severely hampered by the relatively low brightness of Aladdin, which limited the available flux at the microscope's focus and, consequently, the achievable spatial resolution because of signal-to-noise considerations. As a consequence, the experiments at SRC were often forced to operate at a reduced resolution in order to obtain realistic counting rates.

The installation of the microscope on a third-generation light source clearly appeared as the only possible solution to this problem. A participating research team (PRT) was formed for this purpose, and MAXIMUM was moved from Wisconsin to the ALS in April 1995, where it was temporarily installed on bending-magnet Beamline 6.3.2 and preliminary tests were performed. Here we report the successful installa-

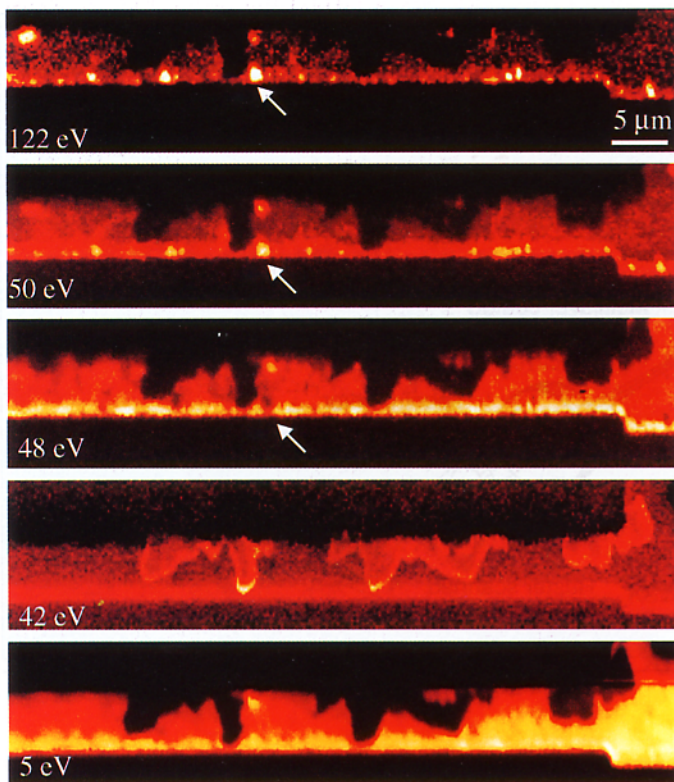


Figure 9: Effects of electromigration on a 5-micron Al-Cu wire. The arrows indicate one of the Cu precipitates.

tion of MAXIMUM at its final location (Beamline 12.0 at the ALS) in 1997. This undulator beamline provides  $1.6 \times 10^{14}$  photons/sec at 130 eV.

Figure 9 shows a set of images taken by MAXIMUM at Beamline 12.0 in an investigation of *in-situ* electromigration (EM) in an Al-Cu wire (see additional discussion in the next section of this article on X-ray micro-diffraction). Extensive void formation is evident in these images. The morphology of the wire is evident in the secondary-electron image at an electron kinetic energy

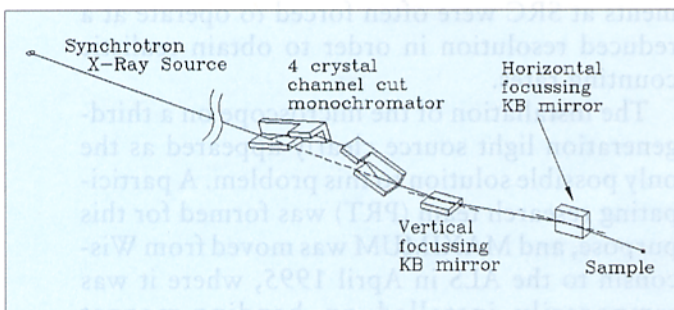


Figure 10. Schematic layout of the K-B mirrors and the four-crystal channel-cut monochromator.

of 5 eV, and the residual aluminum oxide skin in the voids is observed to charge at 42 eV, owing to the electrical isolation from the rest of the line. The copper precipitates (arrows) are clearly seen at 122 eV (Cu 3d), as well as by the contrast reversal from 48 eV to 50 eV, caused by a shift (of about 0.5 eV) of the aluminum oxide core level in Cu-rich regions.

### X-ray micro-diffraction

Kirkpatrick-Baez (KB) mirrors have been developed for the X-ray intermediate energy range (2 keV to 15 keV) [17]. This has allowed progress in the technique of X-ray micro-diffraction. The problem area that best defines the instrumental challenge, matching the capabilities of the ALS is the electromigration problem that affects the semiconductor industry. Electromigration is the physical movement of atoms in aluminum interconnect lines passing current at high electron density (typically in the range of  $10^5$  amp/cm<sup>2</sup>). Significant material movement results in voids that consequently lead to breakage and circuit failure in the metal lines. This problem gets more severe as the line dimensions continue to shrink on integrated circuits.

In spite of much effort in this field [18, 19], electromigration is not understood in any depth or detail, but is strongly associated with the physical material properties (stress and strain) within the aluminum interconnect material. In addition these aluminum wires are buried in an insulating coating (usually SiO<sub>2</sub>). X-rays are ideally suited to probe these buried metallic wires—the requirement being to establish the metallic grain orientation and strain (by measuring small changes in the d spacing) along the wire length. The aluminum grains are typically of the size of about a micron. The instrumental task is to carry out X-ray crystallography on micron-sized samples.

Regular crystallography usually fixes the photon energy and scans the sample angle. If this were carried out with a micron-sized sample and a micron-sized X-ray probe, the sample and X-ray beam would rapidly become misaligned, as the sphere of confusion of regular goniometers is typically tens of microns. We have adopted the alternative approach of fixing the sample position and scanning the photon energy. Figure 10 shows the schematic for the experimental setup. It consists of a four-crystal monochroma-

tor (two channel cuts) at a distance of 31 m from the bending-magnet source, followed by the KB mirrors, which focus X-rays onto the sample. Spot sizes achieved to date are 0.8 micron FWHM. Diffracted X-rays from the sample are detected by an X-ray CCD. The monochromator crystals are mounted off-axis, which allows us to switch between white and monochromatic light while illuminating the same spot on the sample.

The procedure for X-ray micro-diffraction begins with finding the sample. This is achieved by illuminating the grain of interest with white light and monitoring the Laue pattern with the sample to CCD geometry shown in Figure 11. A typical Laue image from an aluminum grain on a silicon (100) substrate is shown in Figure 12. The bright symmetric spots are those of the silicon substrate, but if one looks closely there are several weak asymmetric spots from an aluminum grain misoriented with respect to the silicon substrate. Digitally subtracting the silicon spots results in the Laue pattern shown in Figure 13, which can then be indexed. With the spots indexed, the d spacing of the relevant planes can be measured by switching to monochromatic light and determining the photon energy of the individual Laue spots. The d-spacings have been measured to 1 part in  $10^{-3}$ , which confirmed the indexation. To measure strain within the aluminum grain, d-spacing measurements some 10 to 100 times better are required. This work is under way with the delivery of a new custom-built instrument capable of meeting the angular-stability requirements.

#### Micro X-ray absorption spectroscopy and micro X-ray fluorescence

In order to determine project feasibility for the earth and environmental sciences, we have done initial experiments using high-spatial-resolution determinations of elemental distribution and chemical specificity on a test facility at the ALS using the intermediate X-ray energy range (2 keV to 15 keV). The two techniques, X-ray fluorescence microscopy (XRFM) and micro X-ray absorption fine-structure spectroscopy (microXAFS), provide characterization probes on the micron scale for the study of highly heterogeneous systems [21]. These probes are ideally suited for the study of a variety of scien-

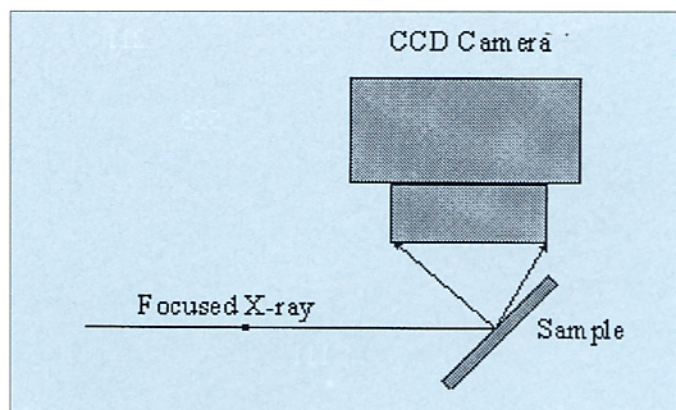


Figure 11. Schematic layout of the sample-CCD arrangement.

tific problems in the earth and environmental sciences that have previously not been possible to address or understand. In addition, the appropriate control of time and experimental conditions will provide mechanistic information and new insight into the interaction of such complex systems. Research areas that could directly benefit from this facility include: transport of nutri-



Figure 12. Laue pattern of a single grain in the aluminum interconnect line with the Laue pattern from the silicon substrate. Time for this exposure was 0.5 sec.

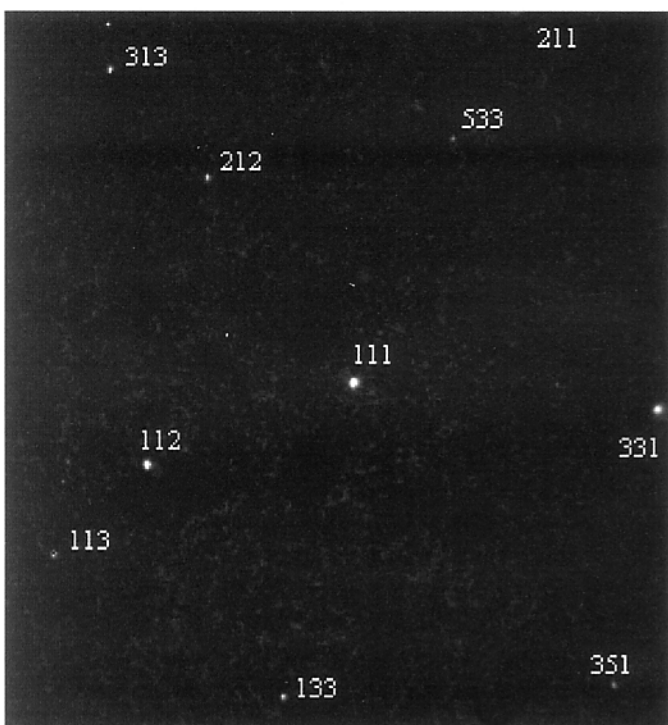


Figure 13. Laue pattern from just the aluminum grain after digitally subtracting the silicon Laue pattern.

ents and contaminants in plants and symbiotic systems; phytoremediation and phytostabilization mechanisms; mobilization of nutrients or contaminants by colloids; mechanism of formation and function of biominerals in plants and animals; and information about diagenesis, climate change, and life forms by the investigation of the latter. Very little detail is known about many of the above systems. This is largely due to the lack of available tools to investigate the systems in their natural environment, using probes that are sufficiently small to investigate the changes on the scale at which they were occurring. We present some initial measurements made on various systems of interest.

The first measurements shown are from an ongoing study, in collaboration with researchers at the Norwegian University of Science and Technology, on the ability of particular fungi to hyperaccumulate certain contaminant metals [22]. We are studying live fungi from the top organic layer of surface soils in the forest lands of southern Norway. These soils are contaminated by a variety of heavy metals (Zn, Cu, Pb, Cd). It is known that the fungi take up and retain

great quantities of the heavy metals, but little is known of the precise forms in which they are retained nor of the mechanisms of uptake and conversion.

Figure 14 shows an optical micrograph of fungi in its natural state (top left). A  $400 \times 400$ -square micron area of interest is marked on the image with the zinc elemental fluorescence map from this area (lower left). This map shows that the Zn is localized in very small regions of dimensions of only a few microns. Also included are a zinc XAFS spectrum taken from a 5-micron region of high Zn concentration along with a spectrum of a zinc-oxalate standard. The signal/noise ratio is sufficiently good to scan some distance into the extended XAFS region, which indicates the potential for extracting structural parameters for this system. In this case a preliminary analysis of the short extended region is consistent with the observation by simple comparison with the very distinctive XAFS from the zinc oxalate standard, that there is a high likelihood that this species is zinc oxalate. In addition, our conclusion supports that of recent work by Sarret et al. using conventional XAFS [23], which showed that, for zinc sequestered by lichen (a symbiotic microorganism consisting of an algae and a fungi) under similar conditions of contaminant exposure, the dominant product is zinc oxalate.

This experiment demonstrates the capability of making a direct species determination on a very small spatial scale. The results suggest that zinc oxalate is an important intermediate in the retention or conversion of Zn by these fungi in their symbiotic relationship with the trees.

We have made preliminary measurements to the study of the kinetics of formation of mixed metal hydroxides on the surfaces of various clays. Recent XAFS measurements made at the National Synchrotron Light Source (NSLS) in studies by Donald Sparks' group at the University of Delaware made an important contribution to the understanding of metal ion retention in the environment [24, 25, 26]. It was found that, under certain conditions of pH and concentration, nickel forms nickel-aluminum hydroxides on the surfaces of a number of clays. These hydroxides are quite resistant to dissolution and less soluble and thus severely reduce the mobility of Ni in the environment. It is thought that the same behavior will apply to a large number of

## Zinc Speciation in Fungus from Contaminated Forest Soils

Optical Micro-graph

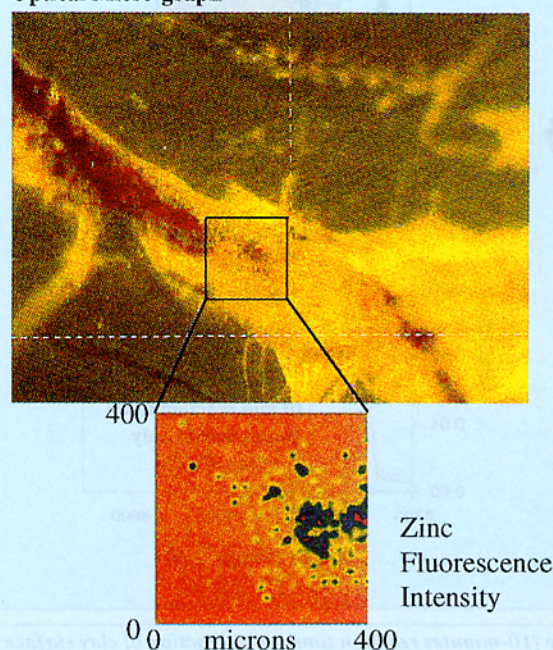
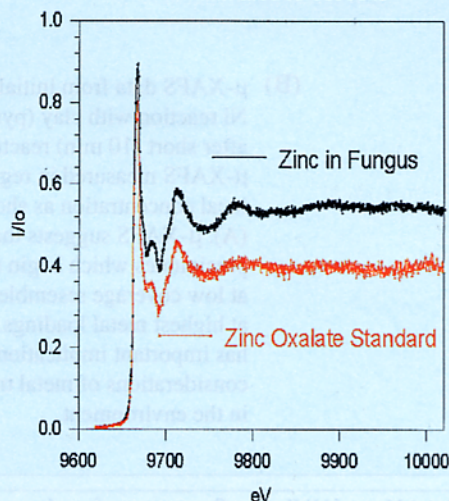
Micro-XANES of 5µm Zinc particle in Fungus  
from contaminated forest soils

Figure 14. Zn-speciation in fungus from contaminated forest soils. A zinc elemental fluorescence maps (lower left) was made from the 400 × 400-square micron area of interest marked on the optical micrograph of fungi in its natural state (top left). This map shows that the Zn is localized in very small regions of dimensions of only a few microns. Also included are a zinc XAFS spectrum taken from a 5-micron region of high Zn concentration along with a spectrum of a zinc-oxalate standard

other metal contaminants, the main criteria being that the ionic radius should be sufficiently close to that of the aluminum cations. In the Ni study, XAFS spectra were taken at various times during reaction of the clay surface with the Ni ions. Despite the clear conclusion that mixed metal hydroxides were forming, it was unfortunately not possible to interpret XAFS data from the low coverages (below 15 minutes reaction time), since the macroscopic concentration was too low and the XAFS data was too noisy.

XRFM measurements of one of the low coverage structures were made at the ALS. These are shown in Figure 15a. It can be seen that some form of Ni aggregation or precipitation is already forming at these short reaction times. It was thus possible to make microXAFS measurements on these precipitates, which appeared to be a few microns in size. These data are shown in Figure 15b, along with data taken using the con-

ventional technique for the longest reaction time (250 hours). These initial data indicate that the precipitates formed at these low coverages are of the same type as those formed at the higher coverages. This suggests that the mixed-metal "binding" of contaminants occurs close to the onset of adsorption, which, in itself, has important implications for metal transport in the environment. More extensive studies are planned [27] in order to check the reproducibility of these initial results. This particular example shows, in the case where there is aggregation and thus local concentration on the micron scale, how microXAFS can be more sensitive than the macroscopic technique and why the parameter describing absorber "dispersion" is more meaningful than the macroscopic value of the concentration.

The last example concerns the ability to directly speciate metals in soils, the most complex of natural systems. The degree of heterogeneity in soils has

### Ni interaction with clay surfaces after short reaction times

(A) Map of Ni K-edge fluorescence for a low coverage phase (10 minutes reaction time of clay surface with Ni ions) showing regions of local concentration of Ni.

(B)  $\mu$ -XAFS data from initial studies of Ni reaction with clay (pyrophyllite) after short (10 min) reaction time.  $\mu$ -XAFS measured in regions of local concentration as shown in (A).  $\mu$ -XAFS suggests that the precipitates which begin to form at low coverage resemble those at highest metal loadings. This has important implications for considerations of metal transport in the environment.

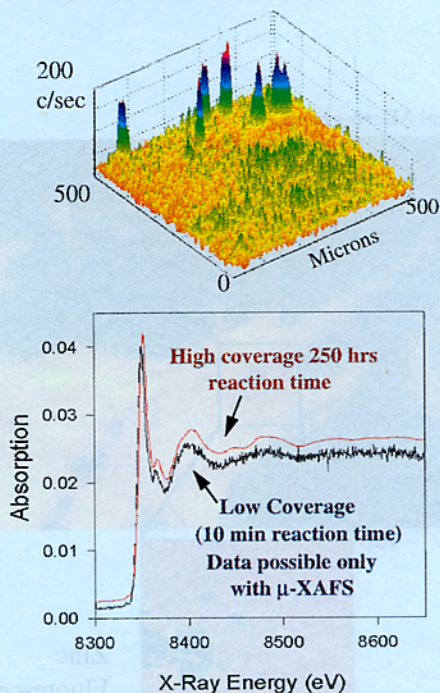


Figure 15. (a) Map of Ni K-edge fluorescence for a low-coverage phase (10-minutes reaction time for interaction of clay surface with Ni ions) showing regions of local concentration of Ni. (b) MicroXAFS data from initial studies of Ni reaction with clay (pyrophyllite) after short (10 minutes) reaction time. MicroXAFS measured in regions of local concentration as shown in Figure 15(a). MicroXAFS suggests that precipitates, which begin to form at low coverage, resemble those at highest metal loadings. This has important implications for considerations of metal transport in the environment.

precluded any direct measurements of contaminant speciation. The most reliable of speciation measurements to date have been made indirectly, for instance by chemical extraction methods (i.e., by applying a series of chemical reagents to infer how the contaminant is bound within the many mineral and organic components of the soil). These indirect methods generally cause alterations to the true soil-contaminant system in the process of trying to make the measurements and are thus notoriously inaccurate.

Figure 16 shows XRFM and XAFS measurements, made during test measurements of a contaminated soil sample from Long Island [28]. The optical micrograph shows the area of interest within a sample of soil contaminated by Cr. The area sampled is  $80 \times 60$  microns. Three elemental maps of Fe and Cr are shown, as determined by X-ray fluorescence. Fe was measured to get an indication of correlations in the metal distributions, if any, as Fe and Mn oxides

are often considered influential in the binding of heavy metals. It can be seen that there is evidence of some correlation between the location of Fe and that of Cr. As can be seen from the elemental maps, the Cr is highly localized (in a region of a couple of microns in size). Significantly, in the case of Cr, we can observe a pre-edge feature that is characteristic of the presence of Cr(VI), which is the oxidation state of greatest concern in terms of its mobility and toxicity.

Speciation using unaltered samples of contaminants in such heterogeneous environments as soils represents one of the most important challenges for environmental analysis. When provided in combination with X-ray fluorescence for elemental analysis, we can additionally monitor the elemental associations of species with particular minerals. Along with knowledge of the species, this determination of the mineral association is also of central importance for devising effective remediation strategies.

### Speciation of Contaminants in Soil at the micron level

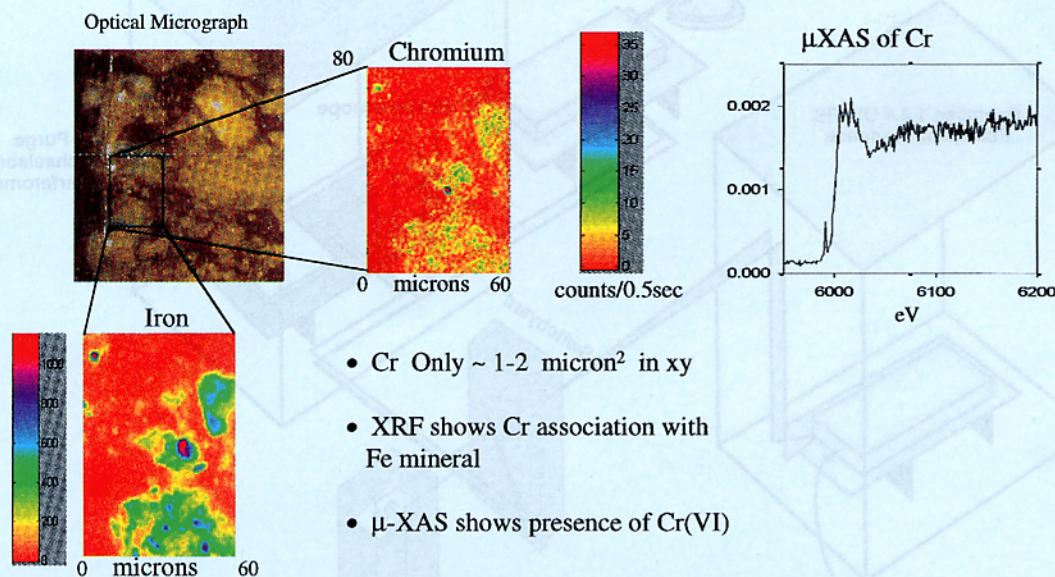


Figure 16. Speciation of contaminants in soil at the micron level. X-ray fluorescence imaging shows the association of Cr with Fe mineral. Micro X-ray absorption demonstrates the presence of Cr(VI).

### FTIR spectromicroscopy

Synchrotron-based infrared (IR) beamlines provide considerable brightness advantages over conventional IR sources [29, 30]. This brightness advantage manifests itself most beneficially when measuring very small samples. In the commissioning of the first IR beamline at the ALS, Beamline 1.4.3, we have experimentally measured the small spot-size obtained by our IR microscopy system when using the synchrotron beam as the source, and we compare it to the internal Globar source. We demonstrate the resolution-limited focus and the corresponding factor of about 100 improvement over conventional sources in measured signal through very small apertures.

Synchrotron light from the Beamline 1.4 bending magnet at the ALS is collimated via a series of aluminum-coated mirrors [31] and is then distributed to one of three end stations, as schematically drawn in Figure 17. Beamline 1.4.3 inputs the light into a Nicolet Magna 760 purged-FTIR spectrometer. The modulated light then passes through a Nic-Plan all-reflecting IR microscope and onto a sample for both transmis-

sion or reflection measurements throughout the mid-infrared region.

To determine the spot-size at the focus of the IR-microscope, the transmission through a 10- $\mu$ m aperture was measured as a function of aperture position on the computer-controlled sample stage. This stage has 1- $\mu$ m spatial resolution, and the FTIR software produces a spectral map of the transmitted light as a function of x and y position of the stage. No other beam-defining apertures were used. The resultant map of integrated IR intensity versus pin hole position is shown in Figure 18. Cuts of the data along the x- and y-directions result in Gaussian line shapes with widths of 10  $\mu$ m in x and 8  $\mu$ m in y. This spot size is becoming diffraction-limited for the low-energy end of our detection capabilities ( $1000\text{ cm}^{-1} = 10\text{ }\mu\text{m wavelength}$ ).

When the above synchrotron measurements are compared to analogous measurements made with a conventional Globar IR source, the brightness advantages of the synchrotron become readily apparent. The Globar has a significantly broader peak profile around 100  $\mu$ m in width simply

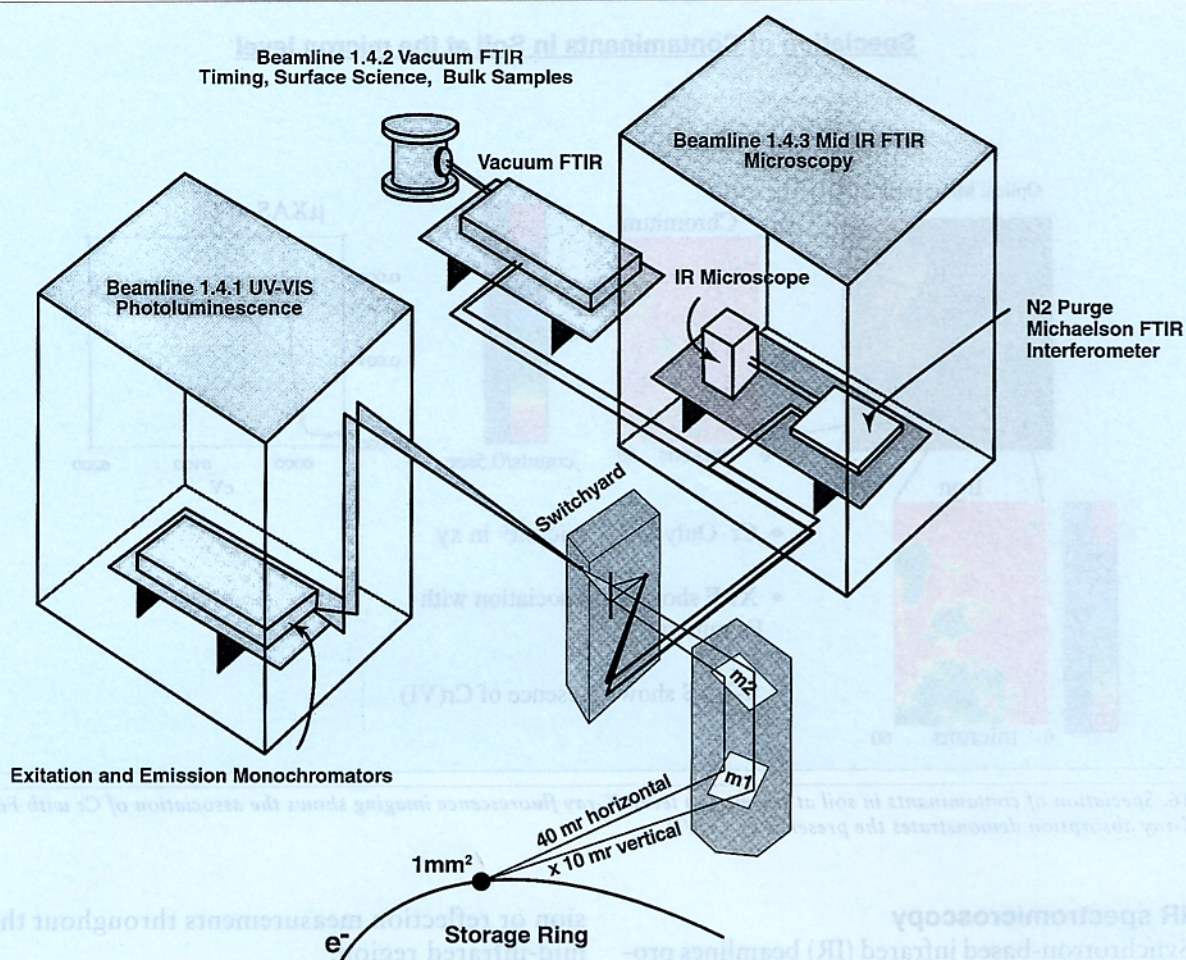


Figure 17. Schematic layout of beamlines 1.4.x at the ALS.  $10 \times 40$  mrad of synchrotron light from the Beamline 1.4 bending-magnet pole is collected and then collimated in the switchyard. The light is then directed to one of three end stations that perform UV photoluminescence, vacuum FTIR, and IR spectromicroscopy, respectively.

because the large source size of this glowing filament source makes a better focus impossible. Therefore, while the overall flux from the Globar and the synchrotron sources is comparable, the synchrotron light can be focused onto a  $10\text{-}\mu\text{m}$  spot. To achieve a similar spot size using the conventional Globar source, one must simply mask the Globar source discarding a large factor of signal intensity. We have measured improvements of a few hundred in intensity transmitted through small pin-holes for the synchrotron source compared to the Globar.

Experimental systems where the sample size is quite small or where features on a sample are on the few-micron size scale will gain significantly by using ALS Beamline 1.4.3. A few examples

include observing bacteria ingesting specific chemicals in real time, localization of adsorbates on environmental surfaces, particulate contamination on semiconductors, polymer laminates and composites, analytical forensic studies of small samples, and measuring materials at high pressure in diamond anvil cells. In summary, synchrotron IR spectromicroscopy enables a host of new scientific pursuits where spectral features can be mapped at the few micron spatial scale. ■

1. PRISM was built by B. Tonner and G. Castro, PEEM2 by S. Anders, M. Scheinfein, H. A. Padmore and J. Stohr.
2. B. P. Tonner, D. Dunham, T. Droubay, and M. Pauli, *J. Electron Spectrosc. Relat. Phenom.* **84** 211 (1997).
3. J. Stohr, *NEXAFS Spectroscopy*, Springer Verlag, New York

(1992).

4. These experiments were performed by S. Anders and Th. Stammler (ALS), H. Ade (North Carolina State University), D. Slep (Hilord Chemical Corp.), J. Sokolov and M. Rafailovich (SUNY@Stony Brook), J. Stohr (IBM), and C. Heske (ALS).
5. S. Anders, Th. Stammler, C. S. Bhatia, J. Stohr, W. Fong, C.-Y. Chen, and D. B. Bogy, Presented at the Material Research Society Spring Meeting, San Francisco, CA, April 13-17, (1998). Proceedings to be published end of 1998.
6. R. N. Watts, S. Liang, Z. H. Levine, T. B. Lucatorto, F. Polack, and M. R. Scheinfein, *Rev. Sci. Instrum.* **68** 3464 (1997).
7. This program originated with a proposal from B. Tonner (Univ. Wisconsin) et al. with continuing development by the ALS.
8. T. Warwick, H. Ade, S. Cerasari, J. Denlinger, K. Franck, A. Garcia, S. Hayakawa, A. Hitchcock, J. Kikuma, J. Kortright, G. Meigs, M. Moronne, S. Myneni, E. Rightor, E. Rotenberg, S. Seal, H.-J. Shin, R. Steele, T. Tyliczszak, and B. Tonner, *J. Synchrotron Rad.* **5** (1998), to be published.
9. E. G. Rightor, A. P. Hitchcock, H. Ade, R. D. Leapman, S. G. Urquhart, A. P. Smith, G. Mitchell, D. Fischer, H. J. Shin, and T. Warwick, *J. Phys. Chem. B* **101** 1950 (1997).
10. S. C. B. Myneni, J. T. Brown, W. Meyer-Ilse, G. A. Martinez, A. Garcia and A. Warwick, Abstracts of the AGU National Meeting, San Francisco, 1997.
11. T. Grundl, S. Cerasari, A. Garcia, T. Warwick, H. Ade, and B. P. Tonner, Compendium of User Abstracts and Technical Reports 1993-1996, Lawrence Berkeley National Laboratory Report LBNL-39981 (1997).
12. J. Kortright, S. K. Kim, T. Warwick, and N. V. Smith, *Appl. Phys. Lett.* **71** 1446 (1997).
13. H. A. Padmore, G. Ackerman, R. Celestre, C.-H. Chang, K.

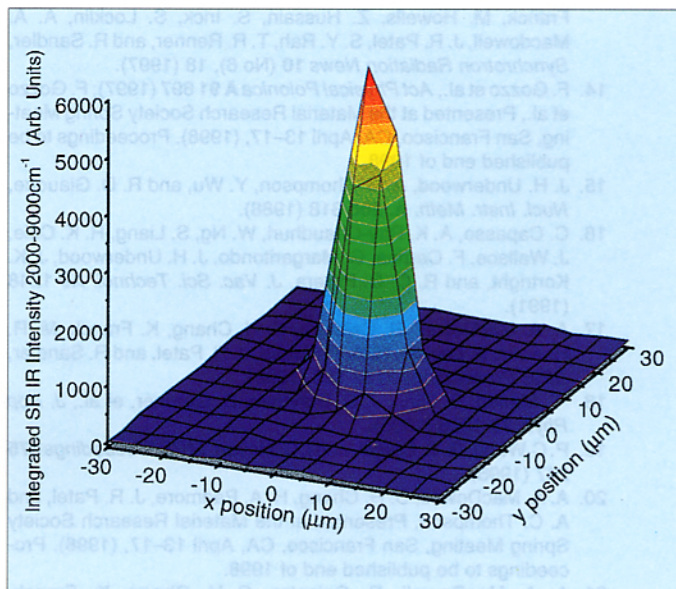
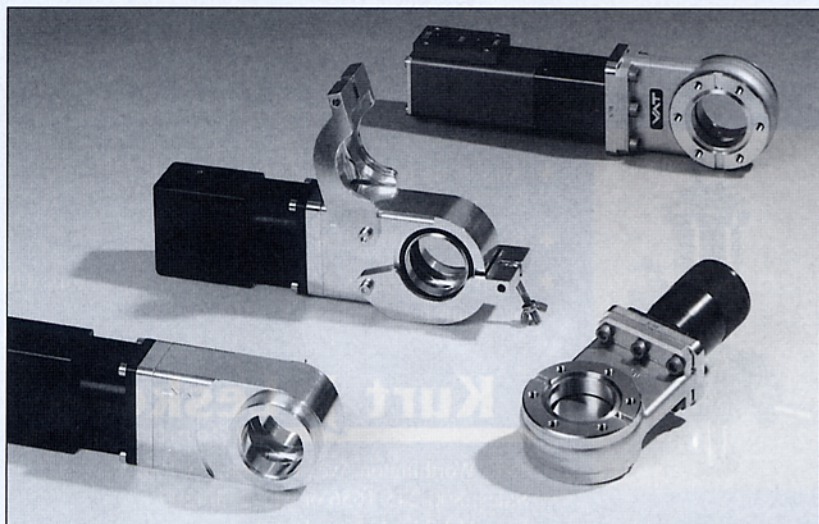


**Figure 18.** Integrated IR signal intensity from 2000  $\text{cm}^{-1}$  to 9000  $\text{cm}^{-1}$  through a 10- $\mu\text{m}$  pinhole being rastered on the IR-microscope stage. There are no other apertures in the optical path. This plot demonstrates the small spot size achieved using the synchrotron IR beam.

## New "Quick Flange" model addition to our Mini Gate Vacuum Valves



Integrated into the valve body are:

- Clamp Assembly
  - ISO Centering & Seal
- Available in sizes 16, 25, 40 & 50 mm I.D.

**Request your new  
Catalog 2000 today**

VAT, Inc., 500 West Cummings Park, Woburn, MA 01801  
Tel 781-935-1446 Fax 781-935-3940  
e mail: [usa@vatvalve.com](mailto:usa@vatvalve.com) <http://www.vatvalve.com>

- Franck, M. Howells, Z. Hussain, S. Irick, S. Locklin, A. A. Macdowell, J. R. Patel, S. Y. Rah, T. R. Renner, and R. Sandler, *Synchrotron Radiation News* **10** (No 6), 18 (1997).
14. F. Gozzo et al., *Acta Physica Polonica A* **91** 697 (1997); F. Gozzo et al., Presented at the Material Research Society Spring Meeting, San Francisco, CA, April 13-17, (1998). Proceedings to be published end of 1998.
  15. J. H. Underwood, A. C. Thompson, Y. Wu, and R. D. Giauque, *Nucl. Instr. Meth. A* **266** 318 (1988).
  16. C. Capasso, A. K. Ray-Chaudhuri, W. Ng, S. Liang, R. K. Cole, J. Wallace, F. Cerrina, G. Margaritondo, J. H. Underwood, J. K. Kortright, and R. C. C. Perera, *J. Vac. Sci. Technol. A* **9** 1248 (1991).
  17. A. A. MacDowell, R. Celestre, C. H. Chang, K. Franck, M. R. Howells, S. Locklin, H. A. Padmore, J. R. Patel, and R. Sandler, *SPIE Proceedings* **3152** 126 (1998).
  18. T. Marieb, P. Flinn, J. C. Bravman, D. Gardner, et al., *J. App Phys.* **78** 1026 (1995).
  19. P. C. Wang, G. S. Cargill, and I. C. Noyan, *MRS Proceedings* **375** 247 (1995).
  20. A. A. MacDowell, C. H. Chang, H. A. Padmore, J. R. Patel, and A. C. Thompson, Presented at the Material Research Society Spring Meeting, San Francisco, CA, April 13-17, (1998). Proceedings to be published end of 1998.
  21. A. A. MacDowell, R. Celestre, C.-H. Chang, K. Franck, M. R. Howells, S. Locklin, H. A. Padmore, J. R. Patel and R. Sandler, *Proc. SPIE*, **3152** 126 (1997).
  22. D. Nicholson, A. Moen, B. Berthelsen, and G. M. Lamb, A. A.

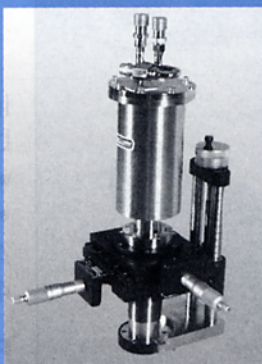
- MacDowell, R. S. Celestre, and H. A. Padmore, ALS Highlights 1997; G. M. Lamb, D. G. Nicholson, A. Moen, and B. Berthelsen, submitted to XAFS X, Chicago, IL, August 1998.
23. G. Sarret, A. Manceau, D. Cuny, C. Van Haluwyn, M. Imbenotte, S. Derulle, and J.-L. Hazemann, Fourth Int. Conf. Biogeochemistry of Trace Elements, June 23-28, 1997, University of California, Berkeley; Geraldine Sarret, PhD these, Observatoire de Grenoble et Laboratoire de Geophysique Interne et Tectonophysique (1998).
  24. Andre M. Scheidegger, Geraldine M. Lamb, and Donald L. Sparks, *Journal of Colloid and Interface Science* **186** 118 (1997).
  25. Andre M. Scheidegger, Geraldine M. Lamb, and Donald L. Sparks, *J. De Physique IV France* **7** c2, 773 (1997).
  26. Andre M. Scheidegger, Daniel G. Strawn, Geraldine M. Lamb, and Donald L. Sparks, *Geochimica et Cosmochimica Acta* (accepted).
  27. Andreas Scheinost, Robert Gale Ford, Geraldine M. Lamb, and Donald L. Sparks (in progress).
  28. R. J. Reeder, G. M. Lamb, A. A. MacDowell, R. S. Celestre, H. A. Padmore, ALS Highlights 1997; ongoing work with Richard J. Reeder, Department of Earth Sciences, SUNY Stony Brook.
  29. Principal investigators: Michael C. Martin, Wayne R. McKinney and Howard A. Padmore, Advanced Light Source, LBNL.
  30. C. J. Hirschmugl, Ph.D. Thesis, Yale University, 1994.
  31. W. R. McKinney, C. J. Hirschmugl, H. A. Padmore, T. Lauritzen, N. Andresen, G. Andronaco, R. Patton, and M. Fong, *Proceedings of the SPIE, "Accelerator-Based Infrared Sources and Applications,"* **3153** 59 (1998).

# Your kind of equation?

$$XYZ + (-196^{\circ}\text{C}) \leq \$16\text{K}$$

The Kurt J. Lesker Company is pleased to announce a new addition to its VG manipulator range: the **Miniax®/Cryotiger®** combination.

APD's Cryotiger® is a low-cost closed-cycle refrigeration unit which will reliably cool large UHV samples to 77K. By combining this unit with Vacuum Generators' Miniax® Low-Cost XYZ Manipulator, the Kurt J. Lesker Company is able to offer a highly effective cryogenic UHV manipulator for about \$16,000.



- \* High Wattage Cooling  
Allows High Cooling Loads
- \* Upgrade for Polar Rotation Available

- \* Motorization Available for XYZ and Polar Rotation  
(with Vacuum Generators' HPT-RX manipulator)
- \* Virtually No Vibration (Cryotiger cooling head has no moving parts)
- \* Allows up to 100mm Z Travel and  $\pm 12.5\text{mm}$  XY Travel
- \* Base Temperature for Cooling: 77K
- \* Resistive Heating Available (with manipulators with 6" mounting flanges)

## Kurt J. Lesker

Company

1515 Worthington Ave., Clairton, PA 15025

Sales: 800-245-1656 or 412-233-4200

Fax: 412-233-4275 sales@lesker.com

international@lesker.com Web: [www.lesker.com](http://www.lesker.com)